



Tissue stretching is a confounding factor for the evaluation of neurodegeneration in the fast-ageing killifish

Steven Bergmans · Pieter-Jan Serneels ·
Luca Masin · Lieve Moons

Received: 6 January 2023 / Accepted: 24 February 2023 / Published online: 13 March 2023
© The Author(s), under exclusive licence to Springer Nature B.V. 2023

Abstract The fast-ageing killifish has gained increasing attention as a promising gerontology model to study age-related processes and neurodegeneration. Interestingly, it is the first vertebrate model organism that shows physiological neuron loss at old age in its central nervous system (CNS), including its brain and retina. However, the fact that the killifish brain and retina are ever-growing tissues complicates studying neurodegenerative events in aged fish. Indeed, recent studies showed that the method of tissue sampling, either using sections or whole-organs, has a large effect on the observed cell densities in the fast-expanding CNS. Here, we elaborated on how these two sampling methods affect neuronal counts in the senescent retina and how this tissue grows upon ageing. Analysis of the different retinal layers in cryosections revealed age-dependent reduction in cellular density but evaluation of whole-mount retinas did not detect any neuron loss, as a result of an extremely fast retinal expansion with age. Using BrdU pulse-chase

experiments, we showed that the young adult killifish retina mainly grows by cell addition. However, with increasing age, the neurogenic potency of the retina declines while the tissue keeps on growing. Further histological analyses revealed tissue stretching, including cell size increase, as the main driver of retinal growth at old age. Indeed, both cell size and inter-neuronal distance augment with ageing, thereby decreasing neuronal density. All in all, our findings urge the ‘ageing science’ community to consider cell quantification bias and employ tissue-wide counting methods to reliably quantify neuronal numbers in this unique gerontology model.

Keywords Killifish · Ageing · Retina · Growth · Cell addition · Tissue stretching

Introduction

In recent years, the African turquoise killifish (*Nothobranchius furzeri*) has gained increasing attention as a strong gerontology model. These fish are characterised by an exceptional short lifespan of only a few months, during which they go through all life-stages (i.e., embryo, larvae, juvenile, adult). Within this short life cycle, the killifish rapidly ages while displaying several hallmarks of human ageing (Kim et al. 2016; Platzer and Englert 2016), previously defined by Lopez-Otin et al. (2013) as a conceptual framework to study ageing (López-Otín et al. 2013).

Luca Masin and Lieve Moons Shared last author.

Supplementary Information The online version contains supplementary material available at <https://doi.org/10.1007/s10522-023-10026-1>.

S. Bergmans · P.-J. Serneels · L. Masin · L. Moons (✉)
Department of Biology, Animal Physiology
and Neurobiology Division, Neural Circuit Development
& Regeneration Research Group, KU Leuven, Leuven
Brain Institute, 3000 Leuven, Belgium
e-mail: lieve.moons@kuleuven.be

The accumulation of these ageing hallmarks, such as cellular senescence, stem cell exhaustion, etc., lead to the development of the commonly described aged phenotype of the killifish, namely skin depigmentation, muscle atrophy, spinal curvature and a decline in both motor and cognitive function (Genade et al. 2005; Cellerino et al. 2016; Kim et al. 2016; Platzer and Englert 2016). Strikingly, the killifish is the first vertebrate model showing physiological neurodegeneration at old age. Indeed, recent observations of naturally occurring Parkinsonian-like dopaminergic cell loss were reported in its central nervous system (CNS), including its brain and retina (Matsui et al. 2019; Vanhunsel et al. 2021; Bagnoli et al. 2022). Therefore, the CNS of this relatively new gerontology model with an extremely fast ageing phenotype might provide crucial insights for neurodegenerative research.

The retina, considered the most accessible part of the CNS, is a well conserved structure among vertebrates, all the way from teleost fish to mammals and thus humans. This layered structure consists of three nuclear layers of neurons: (1) the outer nuclear layer (ONL), containing the nuclei of the cone and rod photoreceptors of which the photo segments reside in the photoreceptor layer (PRL), (2) the inner nuclear layer (INL), where the interneurons (amacrine, horizontal and bipolar cells) are located, and (3) the ganglion cell layer (GCL), that accommodates the retinal ganglion cells (RGCs). These different nuclear layers are separated by two synaptic layers, the outer and inner plexiform layer (OPL and INL), that ensure that electrical cues—converted from incident light—are conducted throughout the retina. The signals are further transmitted to the visual target areas of the brain via the axons of the RGCs that, exiting the retina, form the optic nerve/tract (Stenkamp 2011).

Remarkably, and opposite to its mammalian counterpart, the teleost retina continues to expand throughout life, thereby displaying indeterminate growth, similar to all other teleost tissues and its entire body (Armstrong and Smith 2001). Two main players are known to regulate tissue growth, i.e., cellular addition and tissue stretching (Lyll 1957; Johns 1981; Van houcke et al. 2019). Within the retina, a neurogenic niche, called the ciliary marginal zone (CMZ), is located in the circumferential peripheral region. Both during development and later growth, the CMZ is the main source of cell addition that supports retinal

expansion. This neurogenic region has a specialised spatial organisation of distinct retinal stem cells and progenitors, with the most peripheral edge harbouring the retinal stem cells. This most outer area is delineated by retinal progenitors that become gradually differentiated and finally develop into fully differentiated post-mitotic neurons that are added to the peripheral retina in the different layers according to their lineage (Wan et al. 2016; Fernández-Nogales et al. 2019). As a result of the growth facilitated by the CMZ, over time, concentric circles of newly born cells are added onto the enlarging retina, inducing a radial gradient of cellular age across this nervous tissue (Wan et al. 2016; Fernández-Nogales et al. 2019; Vanhunsel et al. 2021). One cell type that is not produced by the CMZ are the rod photoreceptors, which are generated by another distinct neurogenic niche, the Müller glia (Stenkamp 2007, 2011; Lenkowski and Raymond 2014). These radial glia cells, of which the cell bodies reside in the INL and their processes span across the complete retina, are able to dedifferentiate, divide asymmetrically to form a differentiated Müller glia and a rod progenitor, which will proliferate and eventually differentiate into rod photoreceptors to replace/add rods across the entire retina (Stenkamp 2007, 2011; Lenkowski and Raymond 2014).

Besides cell addition, the teleost retina is known to grow via another mechanism, i.e., through tissue stretching, which, in its most basic description, can be defined as the expansion of existing tissue without addition of new cells (Lyll 1957; Van houcke et al. 2019). Indeed, during the process of stretching, the intercellular space can increase, leading to a reduction of cell density in the stretched tissue (Johns 1981). As nicely illustrated by Van Houcke et al. (2019), retinal tissue stretching can either occur along the axis perpendicular to the retinal layers, leading to thickening of the layers, and/or along the radial plane of the retina, resulting in the increase of the retinal area and subsequent thinning of the layers (Van houcke et al. 2019). One other way of tissue stretching, in which the distance between cell centroids increases but the extracellular spacing remains unaffected, is cell size enlargement (Sands et al. 1979; Dobbing and Sands 1985). Indeed, it is known that tissues and organs in the post-embryonic stage not only develop via cell addition but also through cell growth, thus cell size expansion (Sands et al. 1979; Dobbing and Sands 1985).

The explosive growth of killifish tissues might complicate morphological cell counting, especially when comparing fish at various ages or during different growth phases. A recent study reported neuronal loss in the old killifish brain (Matsui et al. 2019). However, the fact that its CNS is an ever-enlarging organ—regulated by both cell addition and potentially stretching—complicates studying these neurodegenerative events. Indeed, Bagnoli et al. (2022) recently challenged the previously reported loss of both dopaminergic (~25%) and noradrenergic (~75%) neurons in the posterior tuberculum (homologue for the mammalian substantia nigra) and locus coeruleus, respectively (Matsui et al. 2019; Bagnoli et al. 2022). While Matsui et al. (2019) evaluated the number of these tyrosine hydroxylase (TH) immunolabeled neurons using thick brain sections, Bagnoli et al. (2022) studied the TH positive cell densities in whole cleared brains. They observed a significantly lower percentage of cell loss or even the absence of it in certain brain regions (Bagnoli et al. 2022). We recently also reported a decline in dopaminergic cell number in the aged killifish retina upon analysis on retinal sections (Vanhusnel et al. 2021). Within this study, and using a tissue-wide cell counting method, we could no longer confirm this degenerative phenotype. As it is not known how the killifish retina exactly grows throughout life, we next characterised how retinal expansion evolves during ageing and more specifically elaborated on the interplay between cell addition and tissue stretching during adult tissue growth.

Material and methods

Fish husbandry

In this study we only used adult female killifish of the *Nothobranchius furzeri* GRZ-AD inbred strain, as male and female fish of the same age differ tremendously in size, thereby increasing inter-condition variation. Based on in-house lifespan experiments, four adult age groups were defined and used in all experiments, i.e., young adult (6 weeks, w), middle-aged (12 w), old (18 w) and very old (24 w) fish (Vanhoucke et al. 2021). Fish were fed twice a day with brine shrimp (*Artemia salina* nauplii, Ocean Nutrition) during the first two weeks post hatching and then with both brine shrimp and *Chironomidae* larvae

until the age of 5 w. During the later life phases (>5 w), fish were only fed with *Chironomidae* larvae twice a day. Fish were maintained in small (1 L) tanks with a daily water renewal of 50% for the first week, after which they were reared under standardised conditions (temperature 28,3 °C; conductivity 600 µS, pH 7; 12 h light/dark cycle; water renewal 15%) in 3,5 L ZebTec tanks (Techniplast). When the fish reached sexual maturity, they were housed in tanks containing three females and one male, until the age of 12 w, when males were removed due to overdominance. A detailed overview of the housing conditions can be found in supplementary table 1. All animal experiments were approved by the Animal Ethics Committee of the KU Leuven, which strictly follows the European Communities Council Directive 2010/63/EU.

Animal experiments and tissue processing for histological analysis

BrdU pulse-chase

To label new born cells originating from the retinal neurogenic zone, fish were intraperitoneally injected (pulse) with 5-Bromo-2'-deoxyuridine (BrdU, Merck-Aldrich) using a 10 µL Hamilton syringe connected to a 30 gauge needle, all as previously described (Vanhusnel et al. 2021). Briefly, fish were anaesthetized by placing them in tank water containing 0.03% tris buffered tricaine (Merck) and intraperitoneally injected with BrdU solution (8 µg/g body weight). Two injections were performed with a 4 h interval. At 21 days post intraperitoneal injection (dpIP), animals were euthanized, perfused and eyes were collected (chase).

Retrograde biocytin tracing

As there are no antibodies available to label killifish RGCs, we used a retrograde tracing to efficiently and truthfully label retinal ganglion cells (RGCs) (Vanhusnel et al. 2022). Briefly, fish were anaesthetized as described above and positioned on their side under a stereomicroscope. The dermal layer of the cornea was cut and the eye was lifted out of its orbit. Next, the optic nerve was transected at a distance of 0.5 mm from the optic nerve head (ONH) and a wad containing the biocytin (Sigma-Aldrich) tracer was placed on

the proximal end of the nerve. Fish were revived for 3 h, allowing passive transport of biocytin through the RGC axons to their cell bodies in the retina. Following tracing, fish were euthanised, perfused and eyes were collected.

Body size measurement, eye collection and tissue processing

Fish were euthanized using 0.1% tris-buffered tricaine and their body size (length; head to tail) was determined using callipers before performing intracardial perfusion with phosphate buffered saline (PBS, 0.01 M, pH 7.4) and 4% paraformaldehyde (PFA, in PBS, Merck-Aldrich), all as described (Mariën et al. 2022). Eyes were collected and post-fixed for 1 h in 4% PFA at room temperature (RT) and subsequently rinsed three times in PBS. Depending on the follow-up procedure, eyes were either incubated in increasing sucrose solutions (10, 20 & 30% in PBS, Merck) and embedded in 1.25% agarose and 30% sucrose in PBS for cryosectioning, or retinas were dissected and fixed for 1 h in 4% PFA at RT, rinsed three times in PBS and stored in storage buffer (0.4% NaN₃ in PBS) until further use. 10 µm sagittal cryosections were cut using a NX70 cryostat (Epredia), serially collected on eight SuperFrost Plus Adhesion Slides (Epredia) per eye and stored at -20 °C until further use. In all cases retinal orientation (dorsal, ventral, nasal and temporal) was taken into account.

Immunohistochemical stainings

BrdU visualization

New born cells were visualised by staining for BrdU (rat anti-BrdU, Sigma AB6326). Briefly, retinal cryosections of BrdU treated fish were initially dried at 37 °C and hydrated in distilled water (aqua destillata, AD). Next, double-stranded DNA breaks were induced by 30 min incubation in 2 M HCl at 37 °C after which HCl was neutralised by rinsing in 0.1 M sodium borate. Aspecific binding sites were blocked with pre-immune donkey serum before overnight incubation with the primary antibody at RT. Primary antibody was visualized using an Alexa-594 conjugated goat anti-rat secondary antibody and sections were mounted with Mowiol®. Detailed information

concerning primary and secondary antibodies is reported in supplementary table 2.

Biocytin visualization

Retinal cryosections were dried at 37 °C to increase adhesion, after which they were hydrated in AD. Biocytin was visualised using an Alexa 488-coupled streptavidin (1:200, ThermoFisher). Finally, nuclei were stained using 4',6-diamidino-2-phenylindole (DAPI, 1:1000 in PBS, ThermoFisher Scientific) and sections were mounted with Mowiol®.

Retinal whole-mounts (WMs) were initially permeabilized via a freeze-thaw step in 0.5% Triton-X-100 in PBS (PBST) at -80 °C for 15 min. Next, biocytin was visualised using an Alexa 488-coupled streptavidin (1:100) and nuclei were stained using DAPI as described above.

Immunolabeling of amacrine cell types

To evaluate age-dependent cell loss in the INL, immunohistochemical stainings for tyrosine hydroxylase (TH; rabbit anti-TH, Millipore AB152) and choline acetyltransferase (Chat, goat anti-Chat, Millipore AB144P) were performed on retinal cryosections and WMs.

Retinal cryosections were initially dried and subsequently hydrated as described above. Prior to blocking with donkey pre-immune serum, an acid antigen retrieval was performed on samples that were stained for Chat. Primary antibodies were incubated overnight at RT and visualised using Alexa conjugated secondary antibodies (ThermoFisher). Nuclei were visualised using DAPI.

Retinal WMs were initially permeabilized by a freeze-thaw step in 0.5% PBST. Next, an acid antigen retrieval was performed on the samples stained for Chat just prior to blocking with pre-immune donkey serum. TH primary antibody was incubated overnight at RT while Chat primary antibody was incubated for four consecutive days at 4 °C. Finally, primary antibodies were visualised using Alexa conjugated secondary antibodies and nuclei were stained using DAPI.

A detailed overview of the used primary and secondary antibodies is provided in supplementary table 2.

Imaging of (immuno)stained WMs and sections

Entire retinal WMs as well as complete retinal cryosections were imaged with a wide-field epifluorescence microscope (Leica DM6, 20x/0.40 objective) to study BrdU, Biocytin, TH, and Chat positive cell numbers. Per eye, three sections equally spaced on both sides of the midsagittal section containing the optic nerve head (ONH), were imaged for further analysis (max. 240 μm from the ONH), thereby equally representing both the nasal/temporal and dorsal/ventral retina.

To measure the distance between single cone nuclei, the ONL of retinal WMs was imaged based on DAPI signal. Per retinal WM, 12 confocal images were taken using an Olympus FV1000 microscope (Olympus, 60x/1.35 objective), namely three frames (central, C; middle, M and peripheral, P) per retinal quadrant. A schematic overview of how the three frames were sampled is depicted in Figure S3b.

Morphometric analyses

Manual cell measurements

At 21 dpIP injection, BrdU positive cells that were generated by the CMZ and added to the different retinal layers were counted on retinal cryosections using ImageJ in a layer specific way (Figure S1). Six sections per eye were analysed, equally representing both the nasal and temporal retina. To obtain the total number of added cells per section, the BrdU positive cell number—counted on the dorsal and ventral sides of the retina (both present within one retinal cryosection)—were summed. The total number of newly born cells per retina was calculated by summing the total number of added cells. Next, the average number of BrdU positive cells was calculated per fish ($n=6-7$). Similar analyses were done separately for the three retinal layers (ONL, INL, GCL).

TH and Chat positive cells were manually counted on cryosections over the entire length of the INL using ImageJ. Cell counts were performed on six sections per eye and subsequently averaged per fish ($n=10$ for TH; $n=6$ for Chat).

Cell size of TH positive neurons in the INL was studied on predefined areas of retinal WMs stained for TH. Briefly, frames were sampled from retinal WMs at a distance of 160, 745 and 1315 μm from the

optic nerve head, representing the C, M and P frames for each retinal quadrant, respectively. Per frame, the area of ten TH positive cells was measured using ImageJ. Next, the diameter of each cell soma, which was approximated to a circle, was calculated and averaged per frame. Overall, TH positive cell size was evaluated by calculating the average diameter per fish ($n=6$).

Automated cell counting—training, testing and using deep learning counting models

The tissue-wide automated counting models, performed on retinal WMs for all analysed cell types, were repurposed via transfer-learning from RGCode (Masin et al. 2021), and trained following the published pipeline with minor adaptations. Briefly, frames were sampled as described above. The number of frames per dataset and their sizes are reported in supplementary table 3. Ground-truth counts were provided by three independent expert counters. Training frames were equally divided across the three manual counters, while the testing frames were counted in triplicate by all. For transfer learning, the weights of the original RGCode U-Net (Ronneberger et al. 2015) were loaded before starting the training, which was executed until the training loss function reached plateau. The performance of the models was validated on the testing dataset via linear regression and Bland–Altman bias analysis (Figure S2). The slope, coefficient of determination, and bias comparable to the inter-counter values were deemed satisfactory.

Cell counts on retinal WMs were performed by running RGCode with the newly trained models for biocytin, TH and Chat, leading to a total cell number per retinal WM. Next, the average number of counted cells was determined per fish ($n=6-10$ for biocytin; $n=6-10$ for TH; $n=6-9$ for Chat).

Analysis of retinal area—growth rate—and its correlation with body size

Retinal area was measured by manually delineating DAPI stained WMs using ImageJ. Next, the retinal growth rate was determined by the formula stated below. t_2 and t_1 represent two consecutive ages, with t_2 representing the older age group. Of note, when the growth rate was determined for 6 w old fish, retinal area (t_1) and t_1 were considered being zero. This

analysis yielded the growth rate, expressed in mm² per week (n = 11–15).

$$\begin{aligned} & \text{growth rate (t2)} \\ &= \frac{\text{retinal area (t2)} - \text{average retinal area (t1)}}{t2 - t1} \end{aligned}$$

The correlation (Pearson coefficient, *r*) between retinal area and body length was calculated using the build-in correlation analysis method of GraphPadPrism version 9.4.

Analysis of tissue stretching

To evaluate to which extent the retina grows by tissue stretching, the nearest neighbour distance (NND) was calculated using a Python script. The coordinates of all cells centroids per retinal WM were exported from RGCode (Masin et al. 2021). The ONH was manually annotated on every retina using ImageJ. The distance of the five nearest neighbours was calculated for every cell using the *KDTree* function (*k*=5) of the library *scikit-learn* (version 0.22.1). A schematic representation of the NND measurement is shown in supplementary Figure S3a. Moreover, the Euclidean distance between every cell and the optic nerve head was calculated using the *cdist* function of the library *scipy* (version 1.7.3) and rounded to the nearest tenth of a millimetre. The average NND was calculated per fish (n = 4–9).

The distance between single cones was studied based on a concept described in the trout retina by Lyall (1957) as an additional measurement for tissue stretching (Lyall 1957). Distances between four independent single cone nuclei pairs were measured on preselected frames of DAPI stained WMs as described above. A schematic representation is depicted in supplementary Figure S3b. Distances between single cone pairs were only measured when the stereotypic cone pattern was fully intact. Next, the average distance was calculated for each region (C, M, or P) and per WM to evaluate radial and overall stretching per fish (n = 7).

The change in retinal stretching, either in the INL or ONL, between two age groups was determined using the formula stated below. *t2* and *t1* represent

two consecutive ages, with *t2* representing the older age group.

$$\begin{aligned} & \% \text{ stretching (between } t1 \text{ \& } t2) \\ &= \left(\frac{\text{stretching distance } t2}{\text{average stretching distance } t1} - 1 \right) * 100 \end{aligned}$$

Cell size analysis of retinal cell suspensions

To analyse overall cell size in the killifish retina, a single cell suspension was made. Briefly, fish were euthanized using 0.1% tris-buffer tricaine after which the dermal and scleral layer of the cornea were removed, thereby exposing the retina. Of note, while removing the dermal and scleral layer of the cornea, the eye remained in its socket. Next, using sterile PBS, the retinal pigment epithelium was flushed off and both left and right retina were collected in Lebovitz 15 (L15) medium supplemented with 2% Penicillin–Streptomycin (ThermoFisher Scientific), 0,5% Gentamycin (Merck), 2% heat-inactivated Fetal Bovin Serum (ThermoFisher Scientific), 1% Glutamax (ThermoFisher Scientific), 2% MEM Essential Amino Acids (ThermoFisher Scientific), 2% B27 (ThermoFisher Scientific), 25 mM D-Glucose (Merck), 25 mM HEPES (ThermoFisher Scientific) and brought to pH 7.4 (referred to as complete L15, from now). Next, retinas were rinsed three times with complete L15. Sterile activated papain (Antonides) and DNase (ThermoFisher Scientific) were added to the retinas at a final concentration of 16 U/mL and 4.5 U/mL, respectively. Retinas were digested for 30 min at 28 °C, after which they were washed three times with complete L15 complemented with DNase to a final concentration of 4.5 U/mL. Single cell dissociation was accomplished through mechanical trituration in complete L15. Cell clumps were removed using a 40 µm cell strainer (PluriSelect). Cell suspensions were diluted 1:2 with complete L15 to meet cell concentration ranges of the Luna Automated Cell Counter (BioCat). For each fish, cell viability and average cell size were assessed using acridine orange (ThermoFisher Scientific) and the LUNA Automated Cell counter (n = 9–10). The

overall cell survival, cell concentration and cell size are reported in supplementary table 4.

The change in cell size between two age groups (either for the TH + soma diameter or the total retinal cell suspension) was calculated in a similar manner as the “% tissue stretching change” (described above). Here, cell sizes were used instead of stretching distances.

Statistical analysis

All graphs show the individual values and report the mean \pm standard error of mean (SEM). Each graph includes the number of animals used per condition (biological replicates), as indicated by the value *n*. Statistical analyses were performed using GraphPad Prism version 9.4. All raw data passed the Shapiro-Wilco normality test and were tested for parallel equal variance using the Brown-Forsythe test, and found to meet all assumptions in all cases. Significant intergroup differences ($p < 0.05$) were evaluated using an ordinary One-Way ANOVA or Two-Way ANOVA followed by the Tukey’s multiple comparison, and are indicated on the graphs with a different letter. Hence, age groups with a different letter are significantly different from one another while age groups with the same letter do not significantly differ. Additionally, an overview of all *p*-values is reported in supplementary table 5.

Results

All results were obtained using young adult (6 w), middle-aged (12 w), old (18 w) and very old (24 w) female fish of the GRZ-AD killifish inbred strain.

Cell density is artefactually decreased in spatially pre-sampled screenings vs tissue-wide analyses

Considering earlier findings by Matsui et al. (2019) and Bagnoli et al. (2022) that revealed a different cell density in the killifish brain upon 2D (thick brain sections) or 3D tissue-wide (whole cleared brains) analysis (Matsui et al. 2019; Bagnoli et al. 2022), we first compared how spatially pre-sampled 2D analysis on retinal sections correlates to tissue-wide analysis on retinal WMs. Thereto, cell densities of RGCs, dopaminergic and cholinergic amacrine cells were

evaluated on retinal cryosections and WMs, stained for biocytin (after retrograde tracing), TH and Chat, respectively. Analysis on retinal cryosections showed a significant increase in the numbers of both biocytin positive RGCs in the GCL (Fig. 1a), and TH (Fig. 1b) and Chat (Fig. 1c) immunopositive cells in the INL between 6 and 12 w old fish, which can be attributed to retinal growth. Interestingly, the number of biocytin positive RGCs kept on increasing until the age of 18 w, followed by a significant decrease at 24 w. The number of TH and Chat positive cells already stabilised from 18 w of age and were significantly lower during the later life stages as compared to 12 w old fish (Vanhunsel et al. 2021). However, using a well-validated automated tissue-wide analysis method on retinal WMs (Masin et al. 2021), the degenerative phenotype could no longer be observed. Indeed, cell number of all studied cell types—being RGCs in the GCL (Fig. 1d), dopaminergic (Fig. 1e) and cholinergic (Fig. 1f) amacrine cells in the INL—continued to increase until reaching a plateau between 18 and 24 w. Interestingly, the addition rate clearly declined with increasing age for both amacrine populations located in the INL. Altogether, these data clearly show that tissue-wide counting methods are needed to faithfully map cell numbers in the ageing killifish retina and highlight the need to further explore how the retina grows.

The killifish retina keeps on growing throughout life

To evaluate the growth rate of the retina throughout life, we measured the area of retinal WMs from the four different age groups. Scaled images (Fig. 2a) and area analysis (Fig. 2b) revealed that the retinal area clearly expands tremendously between 6 and 12 w old fish ($58.29\% \pm 8.38\%$) and keeps on growing throughout life. Interestingly, there is a high correlation ($r=0.9132$) between retinal area and body length, suggesting a proportional growth. However, although the retina is ever-expanding, the growth rate gradually attenuated with age (12 and 18 w, $21.03\% \pm 7.11\%$; 18 and 24 w, $8.37\% \pm 8.36\%$), highlighting that the older retina loses its exponential growth potential (Fig. 2c). Indeed, while the exponential growth phase of the killifish retina was clearly confined to the early phase (6 w) of adulthood, the retina steadily kept on growing significantly throughout life and its size did not plateau in the studied age window. These findings

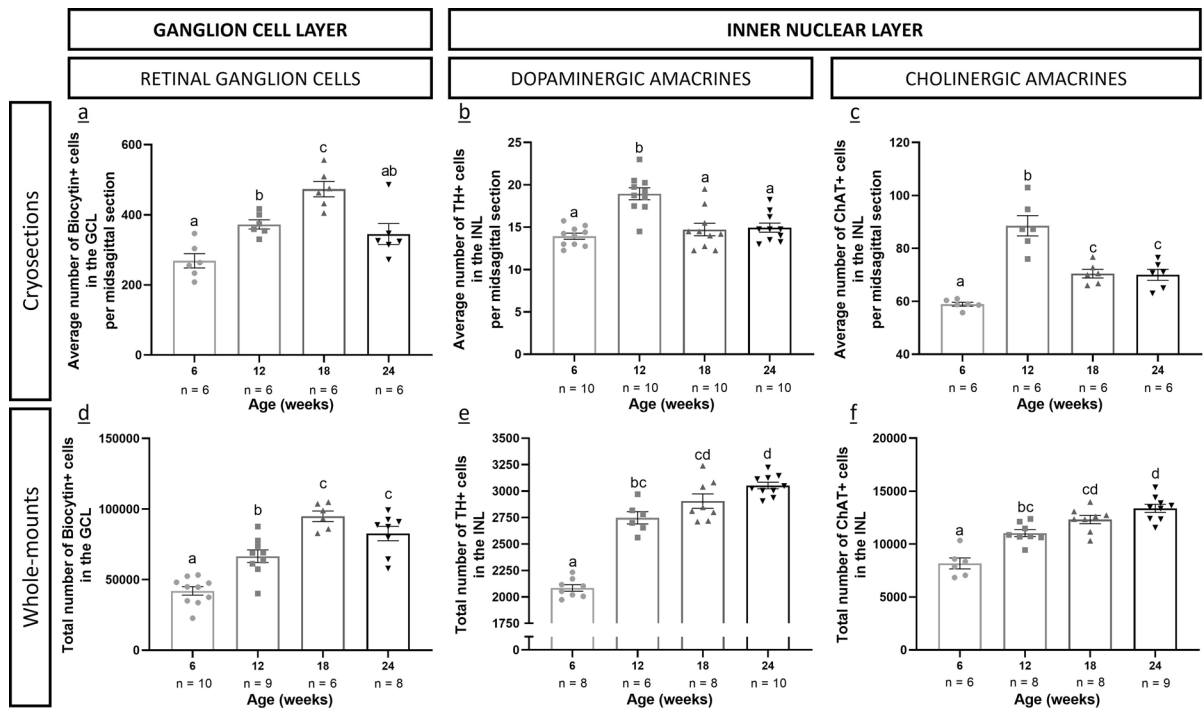


Fig. 1 Cell density artifactually decreases in spatially pre-sampled screenings vs tissue-wide analyses. **a–c** Cell counts for RGCs (**a**), dopaminergic (**b**) and cholinergic (**c**) amacrine on retinal cryosections of killifish revealed an initial significant increase in cell numbers, followed by a decrease upon ageing. **d–f** A tissue-wide analysis method on retinal whole-mounts (WM) did not confirm this growth-degeneration pattern for any of the three cell types. Here, the cell numbers kept on increasing, although addition rates declined with age. All data are presented as mean \pm standard error of mean. Statistical differ-

ences between the age groups are depicted using a different letter and corresponding p-values are reported in supplementary table 5. The number of biological replicates is indicated underneath every condition by the letter n. Of note, cell counts of dopaminergic amacrine on retinal cryosections, shown in panel b, was previously published by Vanhunsel et al. (2021). *Chat* choline acetyltransferase, *GCL* ganglion cell layer, *INL* inner nuclear layer, *RGCs* retinal ganglion cells, *TH* tyrosine hydroxylase, *w* weeks, *WMs* Whole-mounts

raise the question: what is the actual driver of retinal growth during the different phases of life?

Cell addition in the retina decreases with age

The CMZ, the main neurogenic region of the retina located at its periphery, is known to generate retinal neurons throughout life (Wan et al. 2016). To assess how the CMZ, hence cellular addition, contributes to the rapidly expanding retina of the killifish, BrdU pulse-chase experiments were performed (Figure S1). The total number of BrdU positive cells labelled after the BrdU chase was high at young adult age, and significantly decreased upon ageing, stabilising to a very low cell addition rate at 18 and 24 w ($27.49 \pm 5.38\%$ and $18.77 \pm 3.32\%$ of the addition rate at 6 w, respectively) across all retinal layers (total retina, Fig. 3a).

Cell addition levels, measured in a retinal layer-specific way for all age groups, followed a similar pattern across all layers and are almost equally affected by age. In addition, the ratio of new cells added per retinal layer was found to reflect the relative abundance of cells across the different retinal layers, independent of age (Fig. 3b–d), all as previously described for other fish species (Marcucci et al. 2016; Fernández-Nogales et al. 2019). Our results also affirmed the previously reported decline in neurogenic potential of the killifish CMZ (Vanhunsel et al. 2021). Next, when comparing cell addition with retinal area at the four ages, an inverse correlation could be observed for the total retina (Fig. 4a), as well as for the different retinal layers (Fig. 4b–d). Indeed, although the retinal area continued to increase throughout life, cell addition levels reduced very prominently from 6 w of

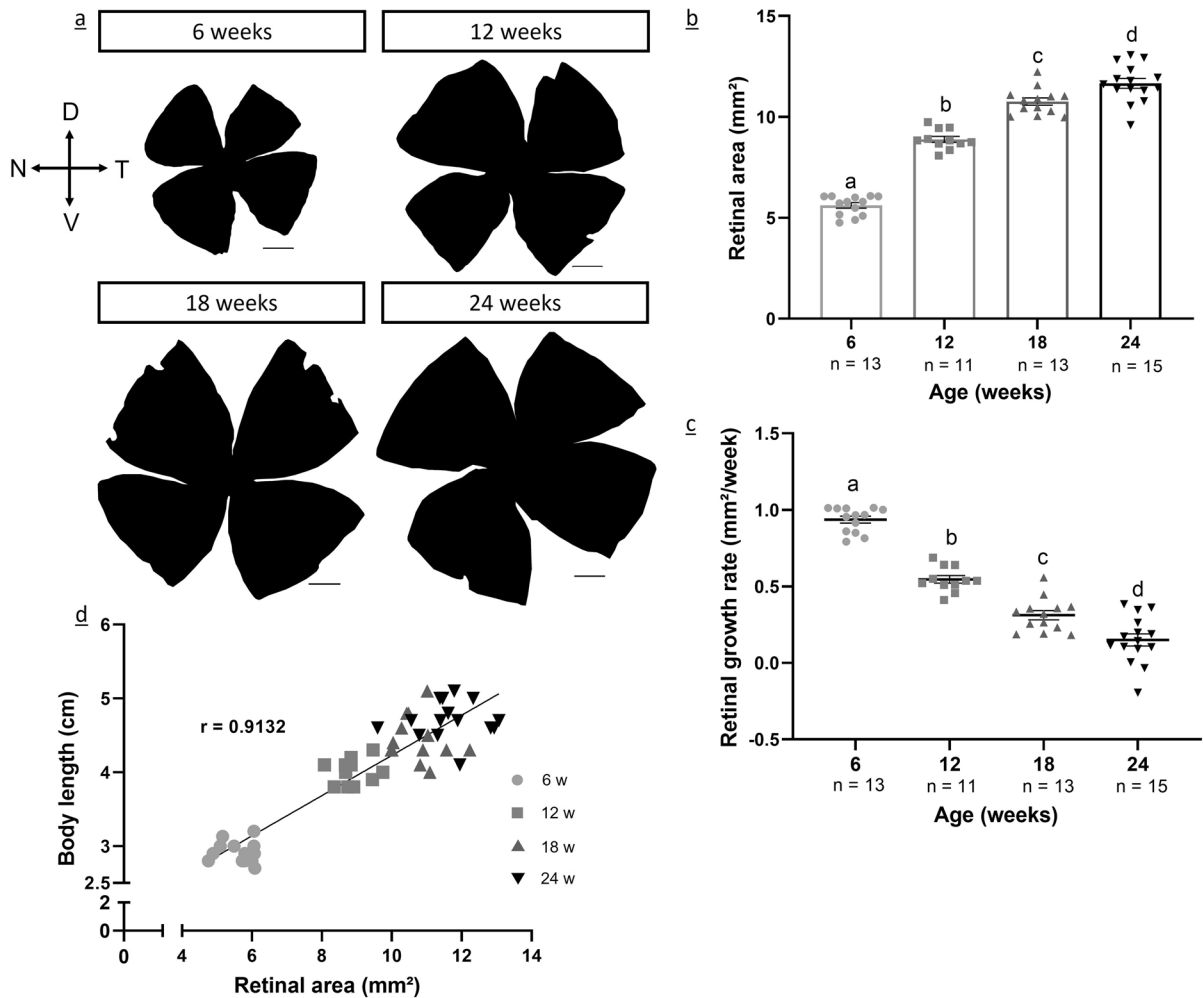


Fig. 2 The killifish retina keeps on growing throughout life. **a** Representative images of retinal WMs clearly showed that the killifish retina continues to grow throughout life. **b** The retinal area of 6, 12, 18 and 24 w old fish significantly increased in all age groups. **c** The retinal growth rate, a measure to study growth in time, significantly decreased in all age-groups. Hence, retinal expansion occurred throughout life with an exponential growth phase in early adulthood that significantly reduced at older age. **d** A high correlation ($r=0.9132$) can be observed between the retinal area (mm²) and the body length

age on. Interestingly, the point of intersection of both retinal area and cellular addition occurred early on in adulthood, i.e., between 6 and 12 w of age. Additionally, a clear positive correlation between cell addition and retinal growth (for all retinal layers) could be observed, as both declined with age (Figure S4). All in all, these findings suggest that next to cellular

(cm) of the killifish. All data are presented as mean \pm standard error of mean. Statistical differences between the age groups are depicted with a different letter and corresponding p-values are reported in supplementary table 5. The number of biological replicates is indicated underneath every condition by the letter n. Of note, the retinal growth rate, shown in panel c, was previously published by Vanhunsel et al. (2021), here, sample size is increased (Vanhunsel et al. 2021). C caudal, N nasal, T temporal, V ventral, w weeks, WMs whole-mounts

addition another mechanism must underlie the continuous growth of the retina at older age.

Tissue stretching is the main driver of retinal growth at old age

Stretching in the plane perpendicular to the retinal layers, or in other words retinal thickening, was

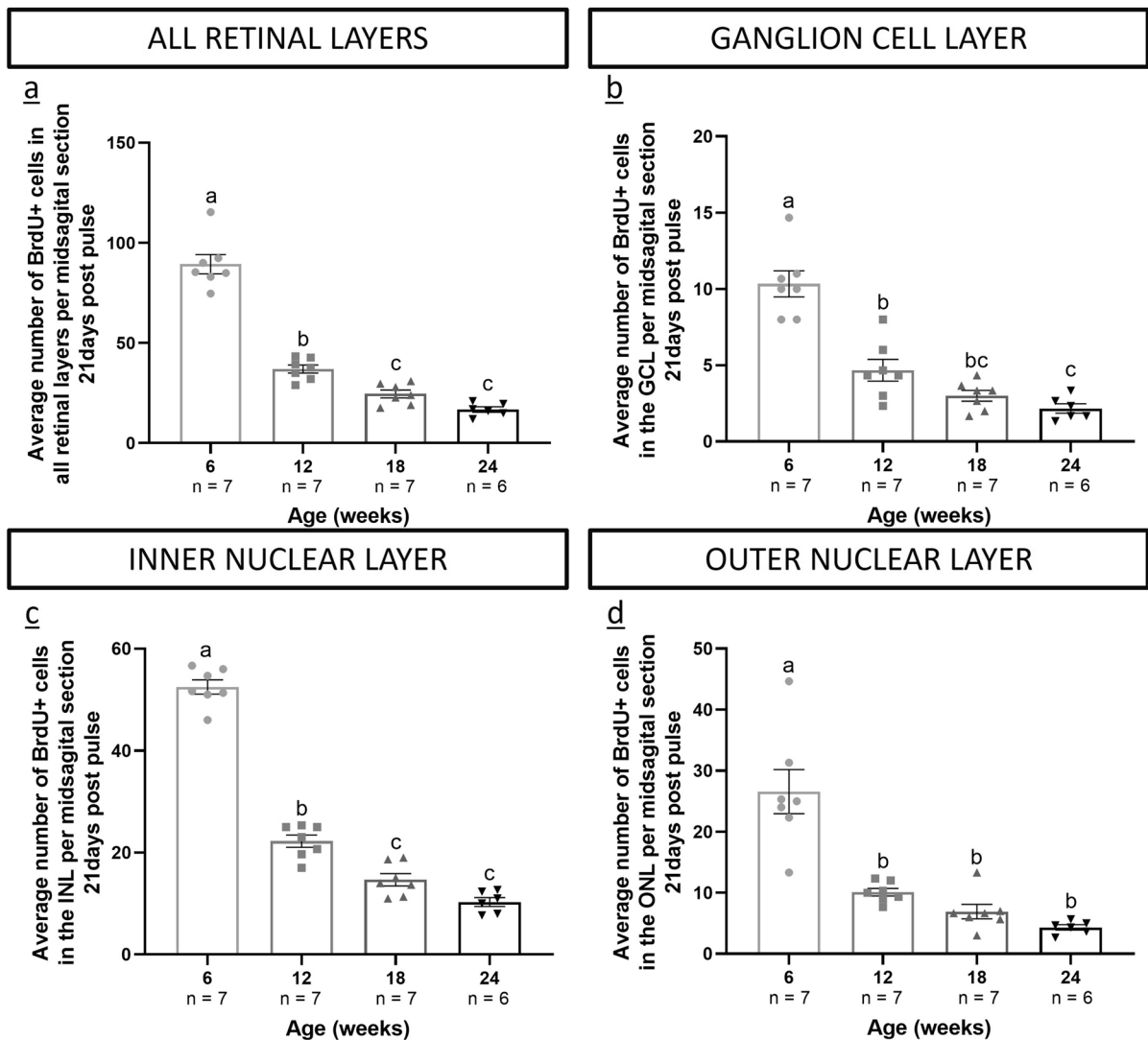


Fig. 3 Cell addition in the retina decreases upon ageing in all retinal layers. **a** Counting of BrdU positive cells within the retinal layers at 21 days after the initial BrdU pulse, revealed a significant reduction in the addition of new born neurons with ageing that stabilized at 18 w with a very low addition rate. **b–d** When focussing on the specific retinal cell layers, being the GCL (**b**), INL (**c**) and ONL (**d**), a comparable pattern could be observed. Interestingly, the number of added neurons seemed to correspond with the relative abundance of neurons across the different layers. All data are presented as

mean \pm standard error of mean. Statistical differences between the age groups are depicted using a different letter and corresponding p-values are reported in supplementary table 5. The number of biological replicates is indicated underneath every condition by the letter n. *BrdU* 5-Bromo-2'-deoxyuridine, *GCL* ganglion cell layer, *INL* inner nuclear layer, *ONL* outer nuclear layer, w weeks. Of note, earlier reported BrdU stained images by Vanhunsel et al. (2021) were re-analysed and sample size was increased (Vanhunsel et al. 2021)

already investigated by Vanhunsel et al. (2021), who disclosed no thickening of the retinal layers, but rather thinning of the GCL, INL and ONL with advancing age (Vanhunsel et al. 2021). These findings could be an indication of either loss of cell/synaptic complexity and/or stretching in the radial

plane of the retina. Therefore, we further elaborated on retinal stretching along this radial axis, which relates to an increase in intercellular space, generally measured as the distance between cell centroids.

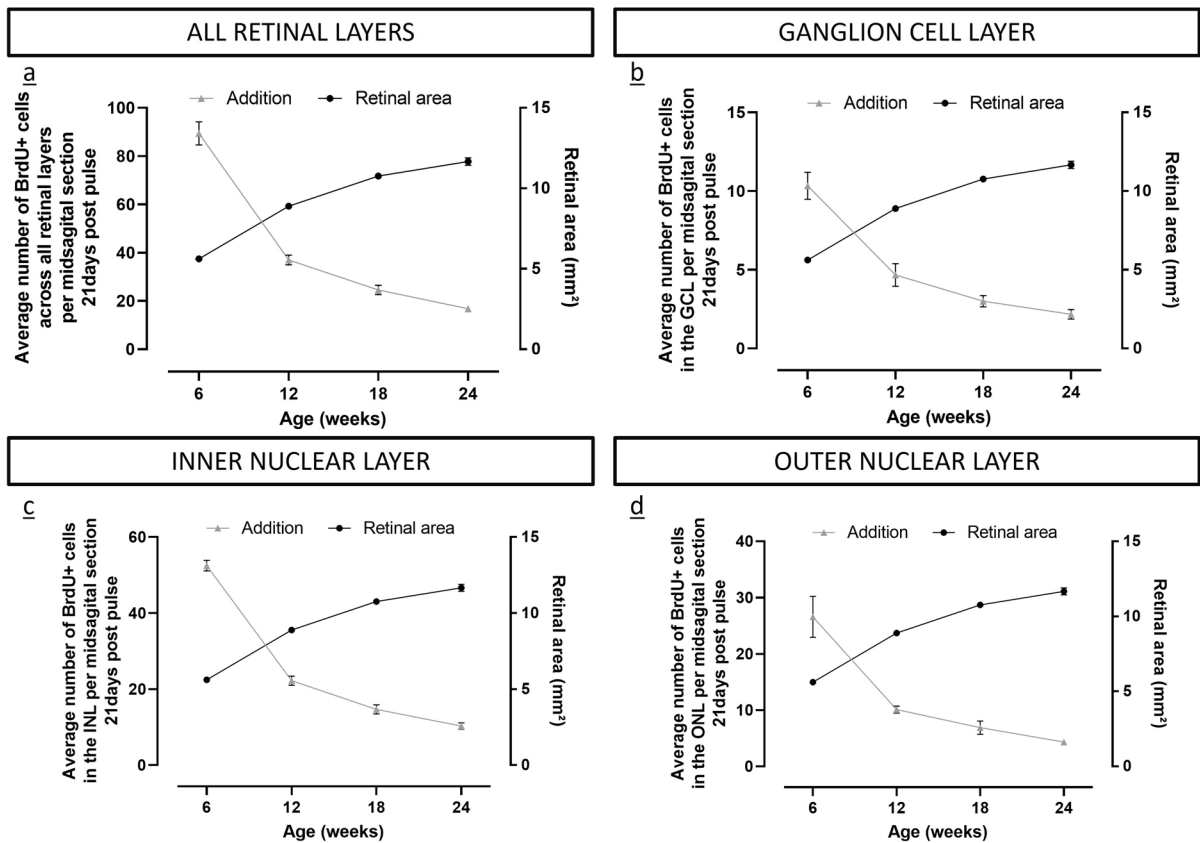


Fig. 4 The inverse correlation between cell addition and retinal area in the fast-growing killifish indicates that addition is not the main driver of retinal growth at old age. **a–d** Plotting both cell addition and retinal area in one graph revealed a point of intersection between 6 and 12 w old fish for the total retina (**a**), as well as for the GCL (**b**), INL (**c**) and ONL (**d**) separately. These data show that in the early phase of adulthood

cell addition is the main driver regulating growth but at older age (from 12 w onwards) another mechanism is at play to support retinal expansion. All data are presented as mean \pm standard error of mean. *BrdU* 5-Bromo-2'-deoxyuridine, *GCL* ganglion cell layer, *INL* inner nuclear layer, *ONL* outer nuclear layer, *w* weeks

Tissue stretching was investigated in the INL by determining the nearest neighbour distance (NND) between TH positive cells on retinal WMs (Fig S3a). While we are aware that potential cell losses could not be excluded using this approach, we sought to minimize their effect by averaging the distance of five neighbours ($K=5$). Our analysis disclosed a very significant increase in the NND of TH positive cells, and thus in INL tissue stretching between 6 and 18 w old fish after which it stabilized (Fig. 5a). An interesting observation was that at the retinal periphery, proximal to the CMZ, the NND of TH positive cells was lowest in young adult (6 w old) fish, indicating that there is a dramatic

post-developmental growth of the retina driven by cellular addition early in the killifish lifespan (Fig. 5b). On the other hand, in fish older than 12 w, intercellular distance was highest at the periphery, suggesting that cellular addition was not able to keep up with retinal enlargement, which thus seems mainly supported by tissue stretching at older ages. Interestingly, at older ages, the intercellular distance increased across the complete retinal radius, including the central retina, which contains cells born prior to the occurrence of extensive stretching. This means that stretching affects the retina along the complete radial component and not only at the periphery.

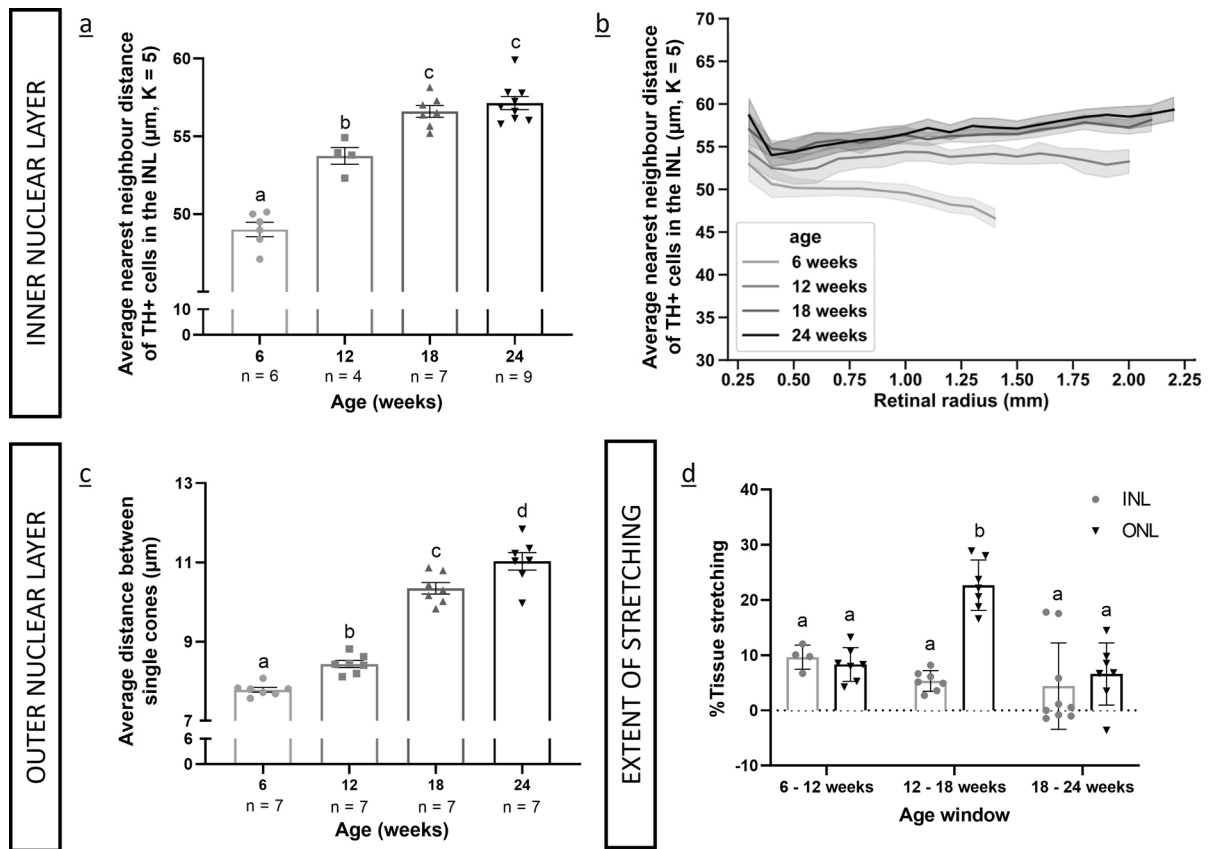


Fig. 5 Tissue stretching is the main driver of retinal growth at old age. **a, b** Analysis of the NND in retinal wholemounts immunostained for TH, revealed that the NND of the dopaminergic amacrine cells in the INL significantly increased upon ageing, plateauing at 18 w (**a**). **b** Interestingly, plotting the NND across the radial distance from the ONH disclosed a clear difference between young adult fish and the older ones. In young adults, the NND was found to be lowest and to decline from the central towards the peripheral retina. As the latter lies close to the neurogenic niche, this data suggest that retinal growth at this age is fully supported by cell addition. The older age groups showed an increasing NND across the retinal radius, which indicated that tissue stretching was the main driver of retinal expansion in older fish **c** The distance between independent single cone pairs was studied using DAPI labelling in the ONL

and this revealed a significant increase in inter-single cone distance, that also stabilised at 18 w. **d** Tissue stretching in the INL seemed to be most pronounced between 6 and 12 w old fish (not significant) while for the ONL the biggest difference in the extent of stretching was observed between 12 and 18 w, data that highlights that stretching is not isometric and thus that different layers stretch in a different way. All data are presented as mean \pm standard error of mean. Statistical differences between different age groups are depicted using a different letter and corresponding p-values are reported in supplementary table 5. The number of biological replicates is indicated underneath every condition by the letter n. p-values are reported in supplementary table. *INL* inner nuclear layer, *K* number of neighbours, *NND* nearest neighbour distance, *ONH* optic nerve head, *TH* tyrosine hydroxylase, *w* weeks

As the stretching process might not be isometric perpendicularly to the retinal layers, meaning that the inner layers with a smaller radius might stretch less than the outer layers with a bigger radius, we also investigated the extent of tissue stretching in the ONL. Here, patterning of the photoreceptors, and more specifically of the cones, conveniently allowed to measure the distance between specific cones, also

as previously described for the trout and zebrafish retina (Lyll 1957; Van houcke et al. 2019). Notably, analysis of this very stereotyped cone receptor patterning enabled us to exclude increased intercellular space due to potential neurodegeneration, a parameter that, although minimised, could not be fully excluded while measuring NND of TH positive cells in the INL. As expected, the distance between single cones

pairs significantly augmented with advancing age (Fig. 5c).

Additionally, when comparing the extent of stretching (%) in the INL and ONL, it could be clearly deduced that stretching is not homogeneous across all ages. While stretching seemed most prominent between 6 and 12 w old fish in the INL ($9.63 \pm 1.90\%$)—although not significant—, in the ONL it was most pronounced in fish between 12 and 18 w ($22.67 \pm 4.23\%$, $p\text{-value} < 0.0001$) (Fig. 5d). Moreover, the increase in intercellular distance caused by tissue stretching persisted at very old life stages (24 w) for the ONL (Fig. 5c), whereas in the INL, it reached a plateau at 18 w (Fig. 5a). Altogether, our data disclose that although cell addition across the different retinal layers follows a similar trend, this is not the case for tissue stretching. All in all, it can be concluded that tissue stretching is highest in young and middle-aged fish (between 6 and 18 w old) when cell addition is lowest, with a clear inner to outer stretching gradient. Hence, tissue stretching is the main driver of tissue growth at later life stages.

Cell size is one of the players underlying stretching

One aspect of cellular stretching that is often overlooked is the increase in cell size itself. Here, we evaluated both the average cell soma diameter of the TH positive cells in the INL as well as the cellular diameter of all retinal cells. Analysis in retinal WMs revealed a significant increase in the TH positive cell soma diameter, which stabilised in fish from 18 w (Fig. 6a). The overall trend of cell size increase was also observed when analysing cell size of all retinal cells using the LUNA Automated cell counter. Retinal cells significantly increased in size between 12 and 18 w old fish, after which this plateaued (Fig. 6b). Of note, while the dopaminergic amacrine cells in the INL seemed to expand most prominently during the early phases of life ($5.76 \pm 1.74\%$), the overall retinal cell size increase seemed to be at its maximum at mid-adulthood ($8.39 \pm 4.9\%$), although not significant (Fig. 6c). Overall, these findings disclose that cell size enlargement is an important contributor to tissue stretching, which is the main driver of retinal growth during the later stages of the killifish lifespan.

Discussion

Being the first model organism to display physiological neurodegeneration at old age, the African turquoise killifish harbours a tremendous potential to revolutionize the field of neurodegenerative and ageing research. Indeed, many findings showing the age-dependent deterioration of the nervous system—such as the accumulation of several ageing hallmarks in the visual system (Vanhunsel et al. 2021), the presence of neurofibrillary tangles (Valenzano et al. 2006) and lipofuscin accumulation (Terzibasi et al. 2008)—potentially leading to the loss of cognitive, motor and sensory functions have steered the community to further explore the degenerative phenotype in the fast-ageing killifish (Valenzano et al. 2006; Terzibasi et al. 2008; Vanhunsel et al. 2021). In the last lustrum, Parkinsonian-like pathology was reported by two independent research groups both showing the aggregation and accumulation of α -synuclein, the main culprit in Parkinson's disease (Matsui et al. 2019; Bagnoli et al. 2022). However, the investigation of cell loss upon ageing, potentially caused by α -synuclein pathology, resulted in contrasting evidence. While Matsui et al. (2019) reported loss of dopaminergic and noradrenergic neurons, Bagnoli et al. (2022) only noticed loss of noradrenergic neurons, and to a much lesser extent (Matsui et al. 2019; Bagnoli et al. 2022). The major difference between these two studies was the method of morphological analysis. While Matsui et al. (2019) used thick sagittal brain sections, Bagnoli et al. (2022) analysed fully cleared brains, thereby excluding the effects of tissue growth on cell density (Matsui et al. 2019; Bagnoli et al. 2022). Their contrasting findings could be explained by the fact that analysis on sections does not consider the tissue expansion perpendicular to the sectioning plane, thereby artefactually increasing cell loss in stretched tissues. Anyhow, these observations suggest that section-confined cell density analysis does not correlate with tissue-wide analysis methods.

While studying how age affects the visual system of the killifish, we also focussed on the degeneration of dopaminergic amacrine cells in the aged retina. Using sagittal sections of the retina we observed an initial increase in cell number between 6 and 12 w old fish that afterwards decreased and eventually stabilised at 18 w, a finding that we initially interpreted as the occurrence of neurodegeneration in the retina

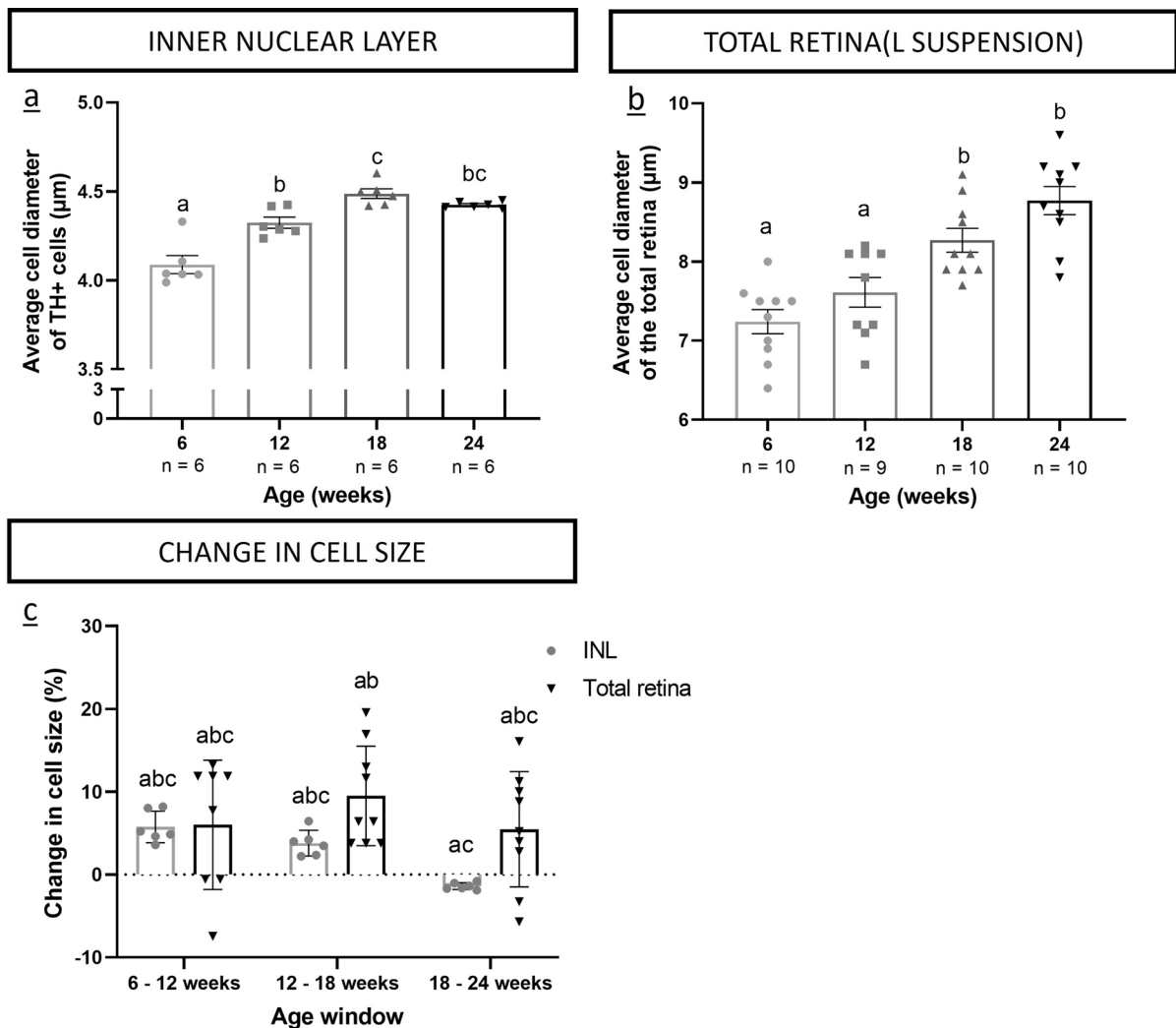


Fig. 6 Cell size increment is one of the processes underlying tissue stretching. **a** Morphological analysis of cell size on retinal whole mounts, immunostained for TH, disclosed a significant increase in amacrine soma size that reached a plateau in 18 w old fish. **b** Assessing cell size in total retinal cell suspensions using a LUNA Automated Cell Counter revealed a similar pattern although a significant increase in overall cell size was only observed between 12 and 18 w old fish, after which it stabilized. **c** Although a trend could be observed for changes in cell size (% of cell size expansion between two age groups) for

both the TH positive cells in the INL and the total retinal cells, no significant differences could be detected, indicating that cell size changes evolve similarly over life time. All data are presented as mean \pm standard error of mean. Statistical differences between different age groups are depicted using a different letter and corresponding p-values are reported in supplementary table 5. The number of biological replicates is indicated underneath every condition by the letter n. TH tyrosine hydroxylase, w weeks

(Vanhunsel et al. 2021). Within this study, we now clearly disclosed that the method of analysis is crucial when evaluating cell number. Indeed, using a tissue wide analysis, we observed that cell number keeps on increasing for several cell types in the inner retina throughout life, reaching a plateau at 18 w of age. These findings indicate that pre-sampled screenings

are not able to recapitulate the biological processes that are ongoing throughout the entire tissue. Therefore, tissue-wide counting methods should become the golden standard in fast-growing tissues/organs/organisms, in order to faithfully map cell numbers and thus possible neuronal loss.

We then also further invested in unravelling how the ever-growing retina of the killifish enlarges throughout life. As expected and in line with findings in other fish species (trout, goldfish, zebrafish), the killifish retina keeps on expanding (Lyll 1957; Johns 1977, 1981; Van houcke et al. 2019). Its growth rate, however, tremendously decreases with age, as was described for killifish body size as well as zebrafish body size and retinal area (Van houcke et al. 2019; Vanhunsel et al. 2021). Of note, these data reflect on how growth is regulated in captivity and thus might differ for killifish in their natural habitat as it has been reported that wild killifish reach sexual maturity, which is highly correlated with growth, within two weeks, as compared to approximately five weeks in captivity (Vrtílek et al. 2018). Indeed, factors such as food supply (limited in the wild), absence of predators in captivity, population density (standardized in captivity) and temperature, impact the growth of wild *versus* captive killifish (Cellerino et al. 2016; Vrtílek et al. 2018). Interestingly, and in contrast to what has been reported in zebrafish, the exponential growth phase of killifish is confined to early adulthood while for zebrafish it is later in life, namely during early to mid-adulthood (Van houcke et al. 2019). These differences in growth regulation between killifish and zebrafish could possibly be explained by a different activity of the CMZ between these two teleost species. Indeed, in zebrafish, the neurogenic potential of the CMZ already decreases in early adulthood (from larvae until 12 months old fish), albeit a substantial number of neurons is still added to the retina at older age (Van houcke et al. 2019). The killifish on the other hand shows an initial hyperactivity of the CMZ, leading to a very high cellular density in the peripheral retina compared to its central part, that supports the initial exponential retinal growth phase in this teleost. This high CMZ activity at young age might then also lead to a depletion and exhaustion of this neurogenic zone early in life, resulting in the very low addition rates observed from 12 w onwards (Vanhunsel et al. 2021). Interestingly, exhaustion of the neurogenic niches reaches beyond the retina, as the stem cell zones of the optic tectum (dorsomedial and ventrolateral zones) have also been reported to become depleted/exhausted upon ageing (Vanhunsel et al. 2021). As such, it is clear that the neurogenic potency is highly affected by age in the entire killifish CNS.

To evaluate how the killifish retina grows in the later phases of life, we determined tissue stretching, as also studied for the zebrafish and trout retina. This phenomenon was investigated using two different methods. For the INL, the NND was determined for the dopaminergic amacrine cells while for the ONL the distance between independent single cones was assessed. The advantage of measuring stretching in the ONL is the stereotypic patterning of the cones, allowing us to exclude the potential degenerative events. While the analysis of tissue stretching in the INL is susceptible to potential neurodegeneration, as there is no stereotyped patterning of the dopaminergic amacrine cells, we tried to minimize this effect by studying the NND between five neighbours. Tissue stretching was found to be most pronounced during the latter phase of retinal expansion when cell addition is lowest, suggesting that retinal growth is mainly supported by stretching during later life stages. These findings are in line with reports in guppy (Müller 1952), carp (Kock and Reuter 1978), trout (Lyll 1957) and goldfish (Johns 1977), where tissue stretching accounts for most of the retinal growth during adulthood. Interestingly, this is not the case in zebrafish, where stretching is the main driver during the early phases of life, while retinal enlargement is mainly facilitated by cell addition from the neurogenic niche(s) at older age (Van houcke et al. 2019). Notably, our results show that tissue stretching is not isometric across the different layers, which can be attributed to the fact that the retinal radius differs for the different layers. For instance, our data disclose that stretching peaks in the INL between 6 and 12 w while in the ONL a maximal stretching can be observed in fish between 12 and 18 w of age. In contrast to studies in other fish species, we also investigated how cell size is affected during retinal growth. Interestingly, for both the dopaminergic amacrine cells as well as for the overall retinal cells, cell size also increases with age, thereby implying it as an important player within the stretching process. Of note, a clear difference in absolute cell size can be observed when comparing total retina cells to the dopaminergic amacrine cells. This can be attributed to both the cell heterogeneity within the total retina, as well as to the use of a single cell suspension for analysis which might have caused minor swelling of the cells.

In conclusion, our findings demonstrate that retinal expansion in the killifish is regulated by cell addition (mainly facilitated by the CMZ) and tissue stretching, including a role for cell size increment. Moreover, there is a specific timing for the two different drivers of retinal growth, being that cell addition initially regulates the exponential expansion during early adulthood while tissue stretching is the main orchestrator of growth at older age. These findings have important implications for neurodegenerative research as section-confined screening methods will not be able to fully account for the effects of tissue stretching on cell densities, especially for organs expanding along the sectioning plane, leading to an artefactual increase in observed cell loss. Therefore, we suggest the usage of 3D tissue-wide screening methods as the golden standard to evaluate cell numbers in fast-growing tissues, such as the killifish brain and spinal cord.

Acknowledgements The authors would like to thank Simon Buys, Arnold Van Den Eynde and Rony Van Aerschot for the daily fish maintenance and environmental control; Stephanie Mentens, Marijke Christiaens and Nele Michiels for their technical support. S.B. and Lu.M hold a personal Research Foundation Flanders (FWO, Belgium) fellowship (1165020N and 1S42720N, respectively). Killifish housing and breeding is financially supported by a small equipment Grant KA-16-00745 (KU Leuven) while experiments are supported by a FWO research grant (G092222N).

Author contributions Conceptualization: SB, LuM and LM; Methodology: SB, LuM, P-JS; Writing—original draft preparation: SB; Writing—review and editing: SB, LuM, P-JS, LM; Funding acquisitions: Research Foundation Flanders, KU Leuven; Visualization: SB, LuM; and Supervision: LM.

Declarations

Conflict of interest The authors have no actual or potential conflicts of interest.

References

- Armstrong HA, Smith CJ (2001) Growth patterns in euconodont crown enamel: implications for life history and mode-of-life reconstruction in the earliest vertebrates. *Proc R Soc B Biol Sci* 268:815–820. <https://doi.org/10.1098/rspb.2001.1591>
- Bagnoli S, Fronte B, Bibbiani C et al (2022) Quantification of noradrenergic-, dopaminergic-, and tectal-neurons during aging in the short-lived killifish *Nothobranchius furzeri*. *Aging Cell* 21:e13689. <https://doi.org/10.1111/ACEL.13689>
- Cellerino A, Valenzano DR, Reichard M (2016) From the bush to the bench: the annual *Nothobranchius* fishes as a new model system in biology. *Biol Rev* 91:511–533. <https://doi.org/10.1111/brv.12183>
- Dobbing J, Sands J (1985) Cell size and cell number in tissue growth and development. an old hypothesis reconsidered. *Arch Fr Pediatr* 42:199–203
- Fernández-Nogales M, Murcia-Belmonte V, Chen HY, Herrera E (2019) The peripheral eye: a neurogenic area with potential to treat retinal pathologies? *Prog Retin Eye Res* 68:110–123. <https://doi.org/10.1016/j.preteyeres.2018.09.001>
- Genade T, Benedetti M, Terzibasi E et al (2005) Annual fishes of the genus *Nothobranchius* as a model system for aging research. *Aging Cell* 4:223–233. <https://doi.org/10.1111/j.1474-9726.2005.00165.x>
- Johns PR (1977) Growth of the adult goldfish eye. III. Source of the new retinal cells. *J Comp Neurol* 176:343–357. <https://doi.org/10.1002/cne.901760304>
- Johns PR (1981) Growth of fish retinas. *Am Zool* 21:447–458
- Kim Y, Nam HG, Valenzano DR (2016) The short-lived African turquoise killifish: an emerging experimental model for ageing. *DMM Dis Model Mech* 9:115–129. <https://doi.org/10.1242/dmm.023226>
- Kock J-H, Reuter T (1978) Retinal ganglion cells in the crucian carp (*Carassius carassius*). I. Size and number of somata in eyes of different size. *J Comp Neurol* 179:535–547. <https://doi.org/10.1002/cne.901790306>
- Lenkowski JR, Raymond PA (2014) Müller glia: Stem cells for generation and regeneration of retinal neurons in teleost fish. *Prog Retin Eye Res* 40:94–123
- López-Otín C, Blasco MA, Partridge L et al (2013) The hallmarks of aging. *Cell* 153:1194. <https://doi.org/10.1016/j.cell.2013.05.039>
- Lyll AH (1957) The growth of the trout reina. *J Cell Sci* 98:101–110. <https://doi.org/10.1242/JCS.S3-98.41.101>
- Marcucci F, Murcia-Belmonte V, Wang Q et al (2016) The ciliary margin zone of the mammalian retina generates retinal ganglion cells. *Cell Rep* 17:3153–3164. <https://doi.org/10.1016/j.celrep.2016.11.016>
- Mariën V, Van houcke J, Arckens L (2022) Intracardial perfusion of the African turquoise killifish. <https://www.protocols.io/view/intracardial-perfusion-of-the-african-turquoise-ki-b2ryqd7w>. Accessed 20 Jan 2022
- Masin L, Claes M, Bergmans S et al (2021) A novel retinal ganglion cell quantification tool based on deep learning. *Sci Rep* 11:702. <https://doi.org/10.1038/s41598-020-80308-y>
- Matsui H, Kenmochi N, Namikawa K (2019) Age- and α -synuclein-dependent degeneration of dopamine and noradrenaline neurons in the annual killifish *nothobranchius furzeri*. *Cell Rep* 26:1727–1733. <https://doi.org/10.1016/j.celrep.2019.01.015>
- Müller H (1952) Bau und Wachstum der netzhaut des Guppy (*Lebistes reticulatus*). *Zool Jahrbücher* 63:275–324
- Platzer M, Englert C (2016) *Nothobranchius furzeri*: a model for aging research and more. *Trends Genet* 32:543–552. <https://doi.org/10.1016/j.tig.2016.06.006>
- Ronneberger O, Fischer P, Brox T (2015) U-Net: Convolutional Networks for Biomedical Image Segmentation. *arXiv*. <https://doi.org/10.48550/arXiv.1505.04597>

- Sands J, Dobbing J, Gratrix CA (1979) Cell number and cell size: organ growth and development and the control of catch-up growth in rats. *Lancet* 314:503–505. [https://doi.org/10.1016/S0140-6736\(79\)91556-3](https://doi.org/10.1016/S0140-6736(79)91556-3)
- Stenkamp DL (2007) Neurogenesis in the fish retina. *Int Rev Cytol* 259:173–224. [https://doi.org/10.1016/S0074-7696\(06\)59005-9](https://doi.org/10.1016/S0074-7696(06)59005-9)
- Stenkamp DL (2011) The rod photoreceptor lineage of teleost fish. *Prog Retin Eye Res* 30:395–404. <https://doi.org/10.1016/J.PRETEYERES.2011.06.004>
- Terzibasi E, Valenzano DR, Benedetti M et al (2008) Large differences in aging phenotype between strains of the short-lived annual fish *Nothobranchius furzeri*. *PLoS ONE* 3:e3866. <https://doi.org/10.1371/journal.pone.0003866>
- Valenzano DR, Terzibasi E, Genade T et al (2006) Resveratrol prolongs lifespan and retards the onset of age-related markers in a short-lived vertebrate. *Curr Biol* 16:296–300. <https://doi.org/10.1016/j.cub.2005.12.038>
- Van Houcke J, Geeraerts E, Vanhunsel S et al (2019) Extensive growth is followed by neurodegenerative pathology in the continuously expanding adult zebrafish retina. *Biogerontology* 20:109–125. <https://doi.org/10.1007/S10522-018-9780-6/FIGURES/10>
- Van Houcke J, Mariën V, Zandecki C et al (2021) Aging impairs the essential contributions of non-glia progenitors to neurorepair in the dorsal telencephalon of the Killifish *Nothobranchius furzeri*. *Aging Cell* 20:e13464. <https://doi.org/10.1111/ACEL.13464>
- Vanhunsel S, Bergmans S, Beckers A et al (2021) The killifish visual system as an in vivo model to study brain aging and rejuvenation. *NPJ Aging Mech Dis* 7:1–17. <https://doi.org/10.1038/s41514-021-00077-4>
- Vanhunsel S, Bergmans S, Beckers A et al (2022) The age factor in optic nerve regeneration: Intrinsic and extrinsic barriers hinder successful recovery in the short-lived killifish. *Aging Cell* 21:e13537. <https://doi.org/10.1111/ACEL.13537>
- Vrtílek M, Žák J, Pšenička M, Reichard M (2018) Extremely rapid maturation of a wild African annual fish. *Curr Biol* 28:R822–R824. <https://doi.org/10.1016/J.CUB.2018.06.031>
- Wan Y, Almeida AD, Rulands S et al (2016) The ciliary marginal zone of the zebrafish retina: Clonal and time-lapse analysis of a continuously growing tissue. *Dev* 143:1099–1107. <https://doi.org/10.1242/dev.133314>

Publisher's Note Springer Nature remains neutral with regard to jurisdictional claims in published maps and institutional affiliations.

Springer Nature or its licensor (e.g. a society or other partner) holds exclusive rights to this article under a publishing agreement with the author(s) or other rightsholder(s); author self-archiving of the accepted manuscript version of this article is solely governed by the terms of such publishing agreement and applicable law.